TEA-2013-0593-ver9-Abbah_1P
Type: research-article

TISSUE ENGINEERING: Part A
Volume 00, Number 00, 2014

DOI: 10.1089/ten.tea.2013.0593

Original Article

AU1 ▶
No gene symbols

Sequestration of rhBMP-2 into Self-Assembled Polyelectrolyte Complexes Promotes Anatomic Localization of New Bone in a Porcine Model of Spinal Reconstructive Surgery

AU2 ▶
AU3 ▶
Sunny-Akogwu Abbah, MD, PhD,[1] Wing Moon Raymond Lam,[1] Tao Hu,[1] James Goh,[1–3] and Hee-Kit Wong, MD[1,3]

Efficient and therapeutically safe delivery of recombinant human bone morphogenetic protein 2 (rhBMP-2) continues to be a central issue in bone tissue engineering. Recent evidence indicates that layer-by-layer self-assembly of polyelectrolyte complexes (PECs) can be used to recreate synthetic matrix environments that would act as tuneable reservoirs for delicate biomolecules and cells. Although preliminary *in vitro* as well as small-animal *in vivo* studies support this premise, translation into clinically relevant bone defect volumes in larger animal models remains unreported. Here we explored the use of native heparin-based PEC, deposited on a hydrated alginate gel template, to load bioactive rhBMP-2 and to facilitate lumbar interbody spinal fusion in pigs. We observed that triple PEC deposits with the highest protein sequestration efficiency and immobilization capacity promoted higher volume of new bone formation when compared with single PEC with low sequestration efficiency and immobilization capacity. This also resulted in a significantly enhanced biomechanical stability of the fused spinal segment when compared with PEC carriers with relatively low protein sequestration and immobilization capacities ($p < 0.05$). Most importantly, PEC carriers showed a more orderly pattern of new bone deposition and superior containment of bone tissue within implant site when compared to collagen sponge carriers. We conclude that this growth factor sequestration platform is effective in the healing of clinically relevant bone defect volume and could overcome some of the safety concerns and limitations currently associated with rhBMP-2 therapy such as excessive heterotopic ossification.

Introduction

NUMEROUS STRATEGIES to utilize bioactive growth factors and cytokines have been explored in different tissue engineering applications. Among this, recombinant human bone morphogenetic protein 2 (rhBMP-2) loaded in solution onto absorbable collagen sponge received regulatory approvals for clinical application in single-level anterior lumber interbody spinal fusion. Although this has produced consistent clinical outcome in many cases, several reports have emerged suggesting that this simplified approach could be lacking in protein delivery efficiency and therapeutic safety.[1] Indeed, although rhBMP-2 is commonly regarded as the most potent bone-inducing molecule in contemporary clinical application, implantation of exceedingly large or ''supraphysiological'' amounts is often reported.[2] The implantation of large amounts of such highly potent proteins could provoke and/or exacerbate adverse tissue reactions and other safety issues associated with rhBMP-2 therapy, including massive soft tissue swellings, respiratory distress, excessive heterotopic ossification, radiculopathy, osteolysis, and possible increase in the risk of malignancies.[1] Therefore, an alternative platform that would ensure delivery efficiency and enhance the safety profile of this and other highly potent cytokines remains an important goal in therapeutic tissue engineering.

From a clinical perspective, adverse tissue reactions and complications such as excessive heterotopic ossification associated with rhBMP-2 continue to limit broader therapeutic acceptance and utilization.[1,3] This has underlined the cautious clinical application of this growth factor in comparison to bone tissue grafts despite the well-demonstrated excellent potency of this biomolecule. rhBMP-2, though cleared by regulatory authorities for limited use in lumbar

[1]Department of Orthopaedic Surgery, Yong Loo Lin School of Medicine, National University of Singapore, Singapore, Singapore. ◀ AU4
[2]Department of Bioengineering, Faculty of Engineering, National University of Singapore, Singapore, Singapore.
[3]NUS Tissue Engineering Program (NUSTEP), National University of Singapore, Singapore, Singapore.

spinal fusion (single-level anterior lumbar interbody fusion [ALIF]), is contraindicated in cervical spinal fusion and several other skeletal reconstructive surgeries.[1] Seeherman *et al.*[4] reasoned that inefficiencies of collagen carriers to maintain physiological concentrations of the bioactive protein (estimated to be 2 μg/kg of normal bone powder) at local implant sites could be the key factor necessitating the use of ''supraphysiological doses'' that have been implicated in the pathogenesis of several of the reported adverse tissue reactions. Therefore, recent developmental efforts, aimed at enhancing rhBMP-2 therapeutic efficacy and safety, have increasingly evolved from simple protein deposition on carrier matrices toward matrix immobilization that could more closely mimic endogenous conditions.[5,6] Nonetheless, successful delivery of labile growth factors in a matrix-bounded state remains a major challenge in large-defect tissue healing.[5,7]

In their native environment, endogenous BMPs and other similar bioactive macromolecules are sequestered to extracellular matrix (ECM) components, including heparin-like glycosaminoglycans (GAGs).[8] In this manner, the ECM molecules play important roles in the stability, storage, and release of growth factors and thereby control their biological activities (including tissue morphogenesis and regulatory activities). Taking inspiration from this endogenous model, a number of researchers have reported the utilization of various ECM molecules to control different aspects of exogenous growth factor therapy, such as modulation of release profiles and localization of bioactivities, protection against proteolytic degradation, and inherent augmenting or adjuvant therapeutics when ECM molecules are coadministered with growth factors.[9–11] In this respect, Zhao *et al.*[10] reported a 20-fold prolongation of BMP-2 half-life in the presence of heparin, resulting in amplification of BMP-2 bioactivity *in vitro* and *in vivo*. Crouzier *et al.*[6] simultaneously incorporated hyaluronan and heparin into multilayered polyelectrolyte films and showed that both loading and release of BMP-2 are modulated by the chemical composition of the polyelectrolyte films. Recently, Macdonald *et al.*[12] employed a chondroitin-based polyelectrolyte film to load BMP-2 and successfully induced ectopic ossification in rats. In our group, we fabricated polyelectrolyte complexes (PECs) using heparin and different polycations to immobilize BMP-2 with particular consideration to the stability and bioactivity of the immobilized protein. We observed that the presence of heparin within PEC substrates was vital for rhBMP-2 bioactivity when used *in vivo* to facilitate posterolateral spinal fusion in rats.[13] Despite these significant efforts in using layer-by-layer self-assembly of polyelectrolytes to harness the potentials of ECM molecules in tissue engineering, one important challenge remained unresolved; the successful application of this concept in the healing of clinically relevant large-tissue-defect volumes is yet to be achieved as far as we know.[7] Therefore, we hypothesize that PEC deposits could sequester sufficiently bioactive rhBMP-2 to promote bone ingrowth and drive complete healing of a clinically relevant bone defect volume in pigs. To test this hypothesis, we adopted the two-segment ALIF model in pigs to evaluate the efficacy and safety of this therapeutic concept. This enables the evaluation of implant dimensions and volumes that could be applicable in humans.[14–16] The main purpose of the present study was to develop a delivery strategy using the self-assembly of PEC-based biomaterial fabrication protocol to efficiently sequester bioactive macromolecules that would safely regenerate bone and heal clinically relevant defect volumes.

Materials and Methods

Alginate microbead fabrication and PEC deposition

All reagents were purchased from Sigma-Aldrich (St. Louis, MO) unless otherwise stated. Ultrapure medium viscosity sodium alginate (PRONOVA UP MVM) obtained from FMC biopolymer was subjected to 5 mrad gamma irradiation before microbead template fabrication to enhance *in vivo* degradation. Calcium-crosslinked alginate microbeads were fabricated from 2% sodium alginate solution that was dispensed as microdroplets into $CaCl_2$ (200 mM) solution with the aid of an electrostatic bead generator (Nisco encapsulation unit Var V1). The bead-fabrication process and the implant scheme were previously illustrated.[17,18] The outer PEC layer was deposited by sequential incubation in 0.1% poly-L-lysine (PLL; MW = 15,000–30,000) solution followed by washing in water and then incubated in 0.5% sodium heparin solution to form single PEC bilayer deposit. Repeat of this cycle of washing, PLL deposition, washing, and heparin deposition allows subsequent PEC bilayer depositions. The microbeads fabricated for this study ranged between 450 and 500 μm in diameter.

Scanning electron microscopy imaging

Microbeads were fixed in 1% glutaraldehyde in sodium cacodylate buffer, dehydrated in graded ethanol, and subjected to critical point drying as routinely required for scanning electron microscopy (SEM). Images of the microbeads were subsequently obtained using a Leo Gemini scanning electron microscope at an accelerating voltage of 20.00 kV and a working distance of 11 mm.

Fourier transform infrared spectroscopy

Alginate microbeads with and without PEC surface coatings were fabricated as earlier. After each polyelectrolyte deposition, microbead sample was washed with double-distilled water and centrifuged. Before Fourier transform infrared (FTIR) measurement, microbeads were freeze-dried overnight, mixed with potassium bromide (KBr), and compressed into a plate for FTIR spectrum collection. FTIR measurements were taken at room temperature by a Fourier transform infrared spectrophotometer (FTIR-8000 series, Shimadzu, Japan).

Zeta potential measurements

To understand the mechanism of PEC-coated alginate microbeads, zeta potential measurements were performed with the Malvern, ZEN 3600 (Worcestershire, United Kingdom). The baseline value of bare-surface calcium alginate microbeads and PEC-coated alginate microbeads was measured in distilled water.

Loading efficiencies and retention capacity

Dimethylmethylene blue (DMB) was used for measurements of sulfated GAG according to published protocols

with slight modifications.[19] Briefly, 2.5 mg of alginate microbeads modified with single, double, and triple PEC depositions were incubated in 20 μL of heparin solution (1 mg/mL). A final volume of 220 μL was attained by adding deionized water and allowed to incubate for 15 min. After centrifugation at 12,100 *g* for 5 min, 50 μL of supernatant was added to DMB working solution containing 10.7 μg of 1,9-dimethylmethylene blue chloride (Polysciences, Warrington, PA) in 55 mM formic acid. The absorbance aliquots from triplicate samples were determined at 520 nm using a Tecan Infinite Plate Reader (Infinite M200; Tecan Group Ltd, Männedorf, Switzerland). A series of heparin solutions of known concentrations were used as standards to calculate the concentration of heparin in the supernatant.

Determining BMP-2 uptake and retention

To measure the amount of rhBMP-2 loaded into PECs, we adopted the enzyme-linked immunosorbent assay method described previously.[17] Briefly, 2.5 mg of alginate microbeads modified with single, double, and triple PEC depositions were incubated in a 200-μL solution containing rhBMP-2 (6 μg) at 4°C for 1 h. Subsequently, all samples were centrifuged and supernatant was collected as earlier. At the end of the experiment, supernatants were subjected to quantitative analysis using a BMP-2 Immunoassay kit (Quantikine DBP200; R&D System, Inc., Minneapolis, MN). Analysis was performed for all PEC deposits (single, double, and triple deposits) in five replicates to determine BMP-2-loading efficiency. For BMP-2-retention capacity, microbeads were further incubated in normal saline (0.90% w/v) at 4°C for 21 days.

Implant preparation and animal surgery

For *in vivo* evaluation, we incubated single and triple PEC-modified alginate microbeads (0.25 g) in a 2-mL solution containing 600 μg of clinical-grade rhBMP-2 (Medtronic Sofamor Danek, Memphis, TN). Each group of microbeads (single or triple PECs) were subsequently loaded manually (using a spatula) into the pores of mPCL-TCP (medical-grade polyepsilon tricalcium phosphate) bioresorbable scaffolds (Fig. 3A) produced by fused deposition modeling (Osteopore International, Singapore, Singapore; www.osteopore.com.sg) to act as spacers or cage devices as commonly practiced in interbody spinal fusion surgeries.[20,21] The mPCL-TCP scaffold used in the present study was customized with a 100% interconnected pore network structure, 0/90 pore layer down pattern, 70% scaffold porosity, 350–500 μm pore size range, and a dimension of $15 \times 12 \times 5\,mm^3$ (Fig. 3A).

Eight male SPF Yorkshire pigs (50–60 kg body weight) underwent lumber discectomy and endplate decortications from the anterior approach as reported previously (Fig. 3B).[21] All animal-related procedures were performed in accordance with the principles of laboratory animal care and were approved by the institutional review committee on the use of laboratory animals. Surgeries were conducted under strict aseptic conditions. The pigs were anesthetized with intramuscular injection of ketamine (15 mg/kg) and maintained with inhalational anesthesia (isoflorane). The eight pigs were divided into two groups (four pigs in each group) for the bi-segmental (L2/3 and L4/5) ALIF surgeries; one group received single-layer PECs and the other received triple-layer PECs as graft implants. Finally, screws and rod fixation were applied to all operated segments to avoid disc implant displacement (Fig. 3B). Postoperative radiographic evaluations were conducted on all animals immediately after wound closure and before euthanasia.

Microcomputed tomography

Bone ingrowth volume and microstructural morphology were evaluated using an X-ray microcomputed tomography (μ-CT) system (SMX-100 CT; Shimadzu, Kyoto Japan). All specimens were scanned at 80-μm resolution with an integration time of 8 ms. Isotropic slice data obtained were used for image reconstruction and rendering employing 3D Studio Max software version 1.2 (Volume Graphics GmBH, Heidelberg, Germany). Volume of interest representing $22 \times 22 \times 22\,mm^3$ voxels was selected and segmented using BoneJ image software for quantitative bone ingrowth parameters.

Histology

Longitudinal sections including the entire length of the implant were selected and processed for hard tissue histology as reported previously.[20] Briefly, the sections were grounded down to a thickness of $\sim 30\,\mu m$, polished and surface-stained with basic fuchsin, and counterstained with methylene blue metachromatic dye.

Biomechanical testing

Nondestructive mechanical testing of harvested segments was conducted following previously reported protocols.[20–22] Briefly, the facet joints were removed leaving the spinous ligaments and posterior elements intact. Segments potted in dental cement at both cephalic and caudal ends were tested at a constant loading rate (1.0°/s) in flexion, extension, right and left lateral bending, and axial rotation using a servohydraulic material–testing system (MTS Mini Bionix 858; MTS Systems Corporation, Minneapolis, MN). A maximum torque of $5\,N \cdot m$ (determined during preliminary test) was applied without applying any compressive preloads. The moments and angular displacements of the free end of each motion segment were recorded. Five consecutive readings were documented with the last two employed for statistical analysis.

Statistical analysis

Data obtained were analyzed by SPSS software package (SPSS, Inc., Chicago, IL). All values are reported as mean ± standard deviation. Unpaired *t*-tests were used to compare mean values among groups. $p < 0.05$ was considered significant.

Results

PEC build-up, protein loading, and release

Confocal laser scanning microscopy (Fig. 1) conducted ◀F1 on a sample of avidin-FITC (model heparin binding protein)–loaded PEC microbeads shows that the protein sequestered from solution formed a ring on the surface of the microbead template. In addition, sequential increase in the

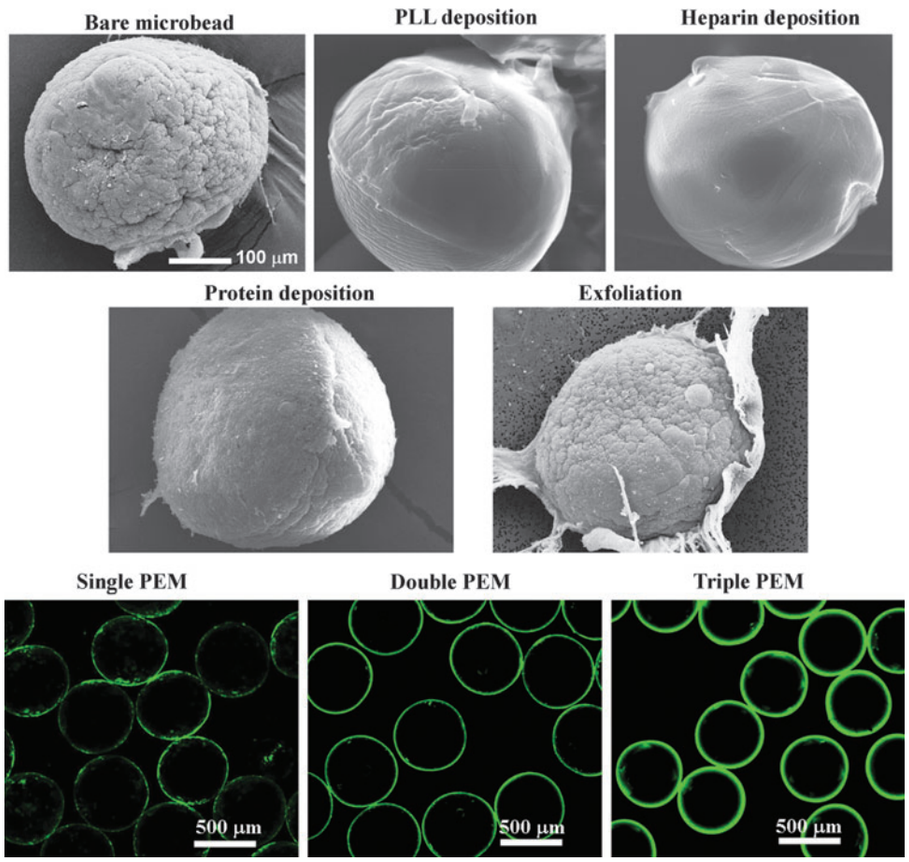

FIG. 1. *In vitro* characterization of polyelectrolyte complex (PEC) fabrication and subsequent sequestration of heparin binding protein from solution. Ultrastructural characterization by scanning electron microscopy (SEM) showed surface topography of a microbead before and after stepwise PEC-protein deposition. A rough-textured topography was observed with bare microbead and a smoothened surface upon polycation deposition. Heparin deposition resulted in egg-shell-like surface while spontaneous protein sequestration converted this shiny surface into a dense, fluffy-wool-coated surface. Notice exfoliation of the fluffy coat that confirms the distinctive PEC-protein deposits on the alginate microbead template. Further evaluation with confocal laser scanning microscopy (using FITC-tagged avidin) enables visualization of the location of protein deposits on the microbeads. Color images available online at www.liebertpub.com/tea

number of alternating PLL/Hep bilayers between 1 and 3 resulted in enhanced localization of the protein as well as increase thickness of the deposited protein layer.

SEM examination revealed topographic changes on alginate microbeads as a result of the sequential loading of different macromolecules (polycation-polyanion-protein) (Fig. 1). We observed a rough-textured topography with formation of grooves, ridges, and pits on the bare surfaces of the microbead templates (attributable to the effects of graded ethanol dehydration/critical point drying SEM procedural requirements). In contrast, PLL (polycation) deposition resulted in a smoothened skinny surface with multiple ''wrinkles'' rather than grooves and ridges. Loading of heparin (polyanion) resulted in further smoothening to give a glossy, egg-shell-like surface with no grooves or wrinkles. Spontaneous loading of rhBMP-2 resulted in a dense fluffy coat. Although a generally intact PEC bilayer (i.e., polycation-polyanion sequential layers) with no evidence of cracking or breakage was consistently observed by SEM prior to protein loading, exfoliation of the PEC-protein deposits from the underlying template was noted in some microbeads after protein loading, particularly among microbeads subjected to multiple cycles of bilayer depositions (Fig. 1).

In vitro *characterizations*

F2 ▶ Zeta potential (surface charge) measurements (Fig. 2A) revealed that calcium alginate microbead templates were initially negatively charged ($\zeta = -20$ mV). Deposition of polycation (PLL) layer drastically changed the surface charges to positive ($\zeta = +40$), while polyanion (heparin) loading completely reverts the surface charges to negative ($\zeta = -50$). The terminal loading of rhBMP-2 considerably neutralized the negative surface charges ($\zeta = -10$). ◀AU5 ◀AU5

We further employed FTIR spectroscopy to confirm the presence of PLL and heparin within the deposited PEC bilayers (Fig. 2B). After coating with PLL, –OH peak intensity and C=O peak intensity decreased due to new interaction between C=O and amine group in PLL molecule (Fig. 2B). Besides, $-CH_2$ peak at 2940 cm^{-1} was observed in the spectrum upon PEC formation. Similarly, absorption of heparin to PLL is reflected by the presence of N-sulfate peak at 1236 cm^{-1}.

Loading efficiencies in this study were defined as the percentage weight of heparin as well as rhBMP-2 in PECs relative to the initial amount in solution, while protein-retention capacity was defined as the percentage weight of rhBMP-2 in PECs on day 21 relative to the initially loaded amount on day 0. Heparin loading as well as protein loading and release analyses (Fig 2C, D) show a nonlinear increase in heparin-loading capacity as the PEC deposition is increased between one and three bilayers. Whereas there was no statistically significant difference in the amount of heparin incorporated into single compared with double PEC bilayers, there was a 1.3-fold increase in heparin incorporated into triple bilayers when compared with single bilayers (Fig. 2). Similarly, a fourfold increase in rhBMP-2-loading

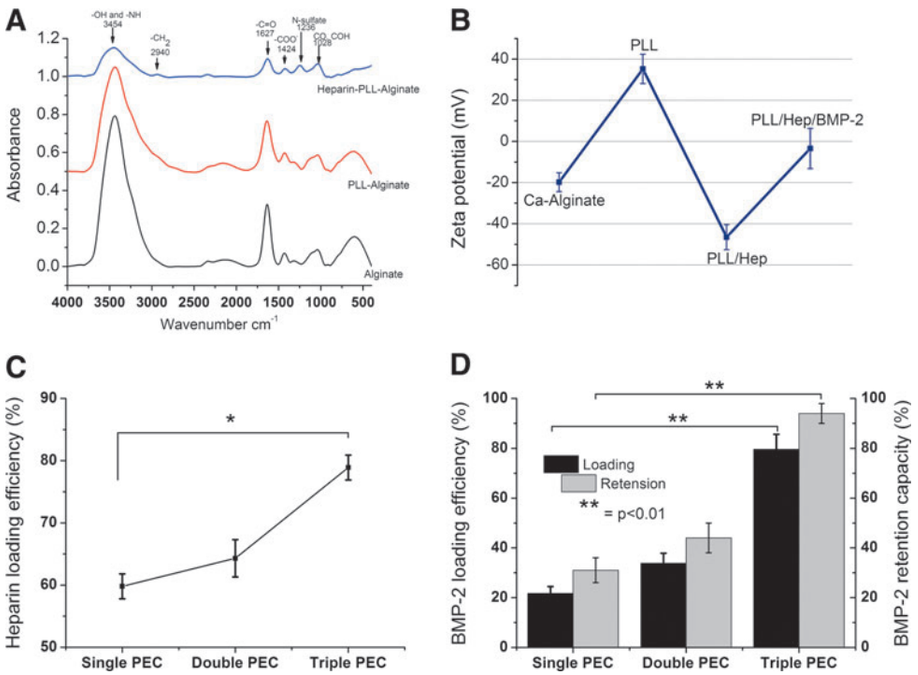

FIG. 2. Characterization of the alginate microbeads before and after deposition of PEC-protein layers using zeta potentials **(A)** and Fourier transform infrared (FTIR) spectroscopy **(B)**. Measurement of heparin-loading efficiency **(C)** as well as BMP-2-loading efficiency and retention capacity **(D)** showed enhancement with sequential increase in the PEC bilayer depositions. Color images available online at www.liebertpub.com/tea

◀AU7

efficiency and immobilization capacity was observed with increasing bilayer deposits (Fig. 2D).

In vivo *osteoinductivity*

For evaluation of bone-regeneration capacity of PEC-bounded rhBMP-2, a two-segment (L2/3 and L4/5) ALIF surgeries were conducted on eight pigs ($n=8$) (Fig. 3B). Bioresorbable mPCL-TCP scaffolds chosen as structural fillers in this study were loaded with either single or triple-layer PEC microbeads (Fig. 3A) and implanted in the prepared disc spaces. Both groups of PEC microbeads were loaded with 600 μg/2 mL rhBMP-2. Results were compared with historical data (mPCL-TCP with 600 μg/2 mL rhBMP-

◀F3

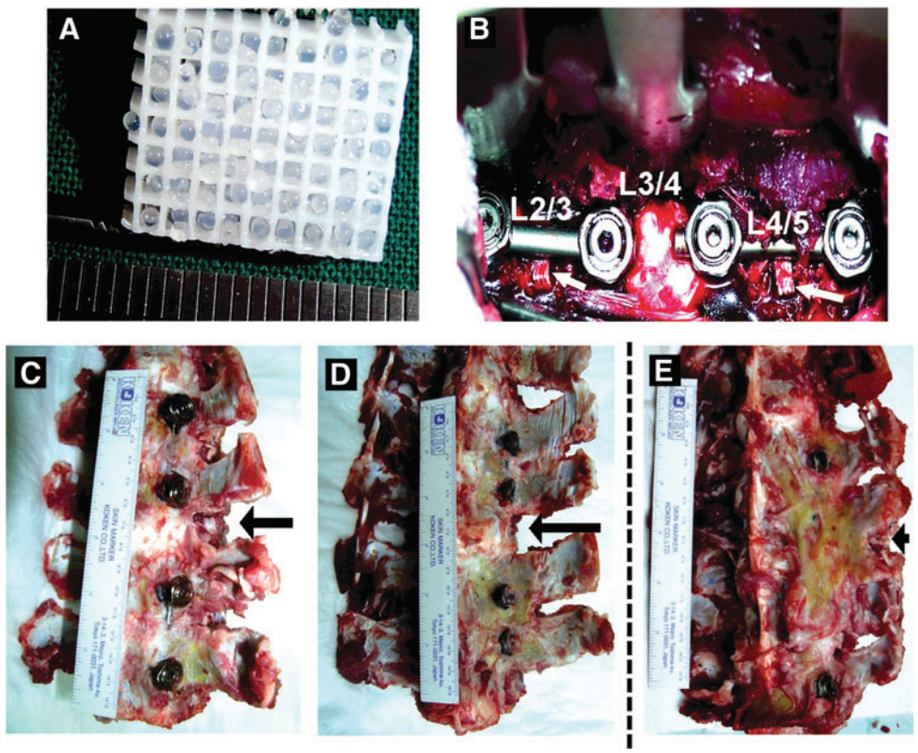

FIG. 3. Gross clinical observations. Upper-panel images are intraoperative photographs showing PEC-laden mPCL-TCP bioresorbable scaffold implant before **(A)** and after insertion into L2/3 and L4/5 disc spaces **(B)** (white arrows). Lower-panel images are harvested lumbar segments. While bone formation was well contained in PEC groups **(C, D)** with no heterotopic bone at the non-operated L3/4 segment (arrow), excessive heterotopic ossification was observed in collagen group inducing fusion of adjacent L3/4 transverse processes and completely burying the two middle screws **(E)**. Color images available online at www.liebertpub.com/tea

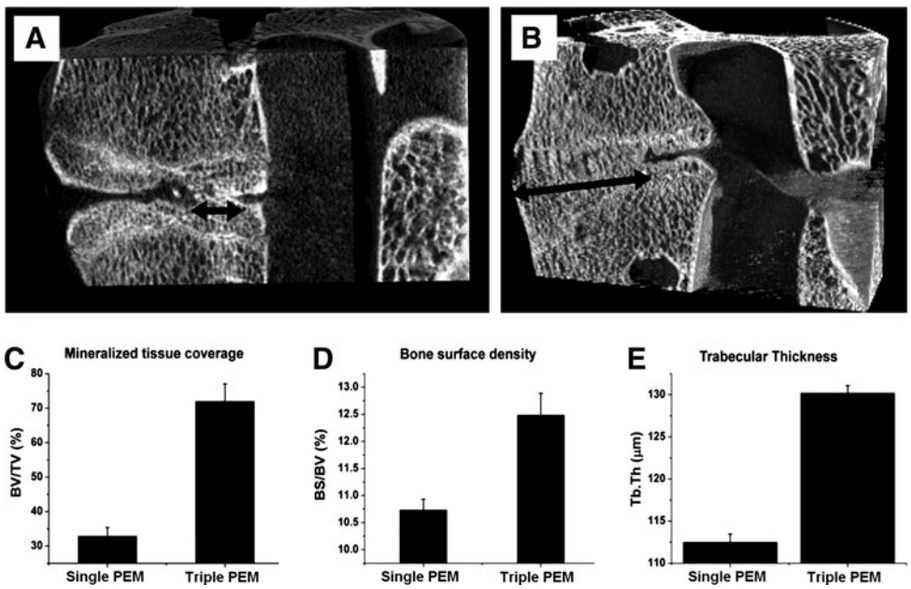

FIG. 4. Three-dimensionally reconstructed micro-computed tomography (μ-CT) images show large-defect spaces in single-PEC implant group **(A)**. In contrast complete fusion was observed in all triple-PEC implant groups **(B)**. Volumetric analysis showed an increase in bone volume fraction, bone surface density, and trabecular thickness in triple-PEC compared with single-PEC implant groups **(C–E)**.

2 delivered on absorbable collagen sponges) in the same animal model.[20]

Gross clinical examination revealed solid fusion in all operated segments with no remarkable differences between single and triple PEC implants when observed by visual inspection and manual palpation (Fig. 3C, D). Compared with historical data for rhBMP-2 (Fig. 3E), a considerably enhanced containment of the newly formed bone tissue within the interbody implant region was noted in both single- and triple-PEC carriers than in absorbable collagen sponge carriers.[20]

μ-CT revealed morphologic and volumetric differences between the two PEC matrix carriers with respect to bone-induction abilities (Fig. 4A–E). While complete interbody spinal fusion was observed in all segments implanted with triple-PEC matrix, only partial fusion was observed in the single-PEC matrix group at 6 months ($n=8$). Similarly, the bone volume fraction was significantly increased in triple-PEC compared with single-PEC group ($p<0.05$). Although percentage volume of bone tissue differed significantly between the two implant groups, the differences in both the

◀F4

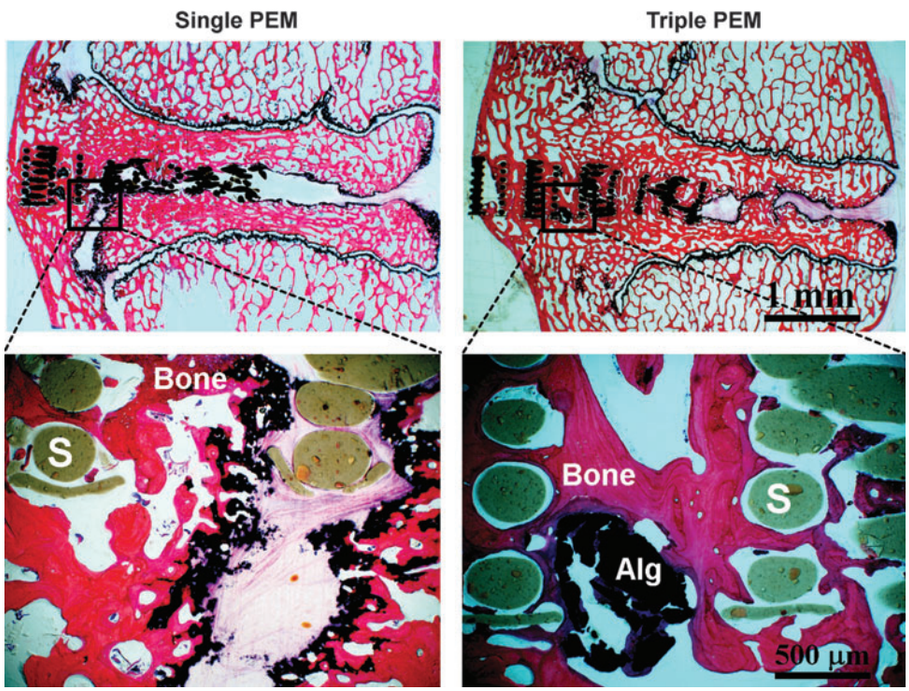

FIG. 5. Calcified-tissue histology (sagittal view) showing bone ingrowth into operated disc spaces in both single- and triple-PEC groups. Notice the light-blue-stained fibrous tissue surrounding some filaments of mPCL-TCP bioresorbable scaffolds (S), suggesting pseudoarthrosis with single PEC. Fragmentation of scaffold filaments was also observed in single-implant groups as opposed to triple-implant groups. Remnants of alginate microbeads (Alg) could still be observed in some segments. Slides were stained with basic fuchsin and counterstained with methylene blue. Color images available online at www.liebertpub.com/tea

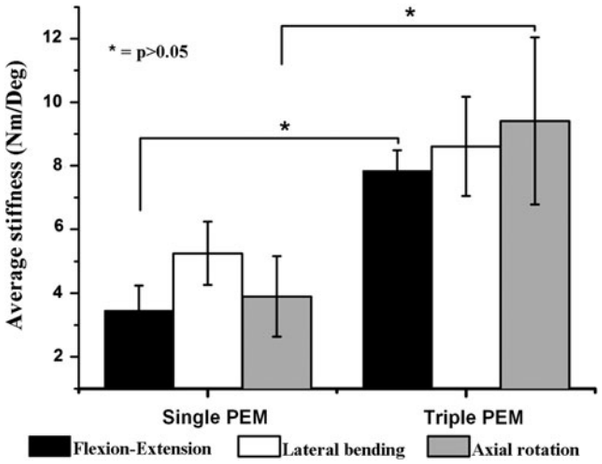

FIG. 6. Biomechanical stability evaluations of operated spinal segments show increase in stability in triple–PEC-compared with single-PEC-treated segments (*$p < 0.05$; ** < 0.01).

bone surface density and trabecular thickness were not statistically significant, indicating that bone quality in both groups was micro-structurally comparable (Fig. 4C–E).

Histology confirmed the ingrowth of bone tissue into the pores of mPCL-TCP in both single- and triple-PEC groups (Fig. 5). Bone induction was by direct rather than endochrondral ossification in both groups. While bone tissue completely bridged the defects in the triple-PEC group, only partial bridging of operated defect spaces and infilling of implanted mPCL-TCP pore network structure was observed with single-PEC implant groups. Higher magnification images showed evidence of soft tissue deposition around some mPCL-TCP struts only in the single-PEC implant group. This finding suggests that insufficient amount of sequestered rhBMP-2 in the single-PEC group predisposes to pseudoarthrosis, further indicating that triple PEC is functionally superior in delivery efficiency compared with single PEC in this model.

Biomechanical evaluation showed statistically significant differences in segmental stability between single- and triple-PEC implants in flexion and extension, lateral bending, and axial rotation (Fig. 6).

Discussion

In this study, we hypothesized that PECs deposited on alginate microbeads could sequester bioactive rhBMP-2 and promote bone ingrowth that will drive complete healing of a clinically relevant bone defect volume in pigs. Our results reveal complete defect healing only when triple-layered PEC deposits with an enhanced growth factor sequestration and immobilization capacity were used to deliver rhBMP-2. By contrast, single-layered PEC matrices with relatively low growth factor loading efficiency as well as immobilization capacity showed inferior histological and functional fusion performances despite using equivalent amounts of rhBMP-2 (i.e., 0.6 mg rhBMP-2).

Interestingly, this same dose of rhBMP-2 (0.6 mg), delivered with collagen sponge, has been previously shown to induce complete interbody spinal fusion in this porcine ALIF model.[20,23] However, excessive heterotopic bone formation was reported with collagen carriers, consistent with clinical observations.[1,20] This resulted in the fusion of adjacent nonoperated spinal segments (L3/4), extending the fusion beyond the intended anterior interbody (intervertebral disc space) portion into the posterolateral, inter-transverse portion of the spinal column (Fig. 3). Among PEC carriers, however, bone formation was localized and largely contained within operation sites in both single- and triple-layered PECs. This observation is consistent with our previous finding of controlled and contained new bone tissue deposition in rat posterolateral spinal fusion studies with PECs as opposed to collagen carriers.[13] Further evidence of new bone containment in this large-animal ALIF model was obtained via 3D reconstructed μ-CT images viewed from the axial projection showing large bone tissue deposition extending anteriorly beyond the implanted scaffold in collagen as opposed to PEC carriers (Fig. 7). Besides, closeup inspection of the scaffold implant region shows an orderly morphological pattern of new bone deposition in both single- and triple-PEC groups with distinctive squares that replicated the pore structure of mPCL-TCP. When compared to collagen sponges loaded into mPCL-TCP, the morphological pattern of new bone deposition was less orderly, presenting a mesh of thin, profuse, and fragile-looking bony trabeculae akin to previous reports.[24–26]

Injection of double-fluorochrome tracers (calcein-green injected 4 weeks postoperatively and alizarin-red injected 8 weeks postoperatively) enabled the localization of osteoid tissue deposition and revealed differences in bone deposition patterns between PEC and collagen carriers (Fig. 8). Whereas newly deposited mineralized tissue was formed along the borders of mPCL-TCP struts as well as in the pore spaces in the PEC carriers, mineralized tissue deposition in collagen carriers was rather diffuse and mainly located in the pore spaces of mPCL-TCP. Controlled and prolonged release of rhBMP-2 from PEC carriers ensured a more orderly new bone deposition in contrast to uncontrolled bolus release associated normally with collagen carriers.

Additionally, almost all the implanted alginate microbeads had degraded over the 6-month implantation period with only scanty remnants observed on histology (Fig. 4). More importantly, there was no evidence of adverse tissue reactions and peri-implant complications, such as chronic inflammation, implant rejection, fibrous tissue encapsulation, or massive cellular infiltration. In addition, implant regions with abundant bone ingrowth into the pores of mPCL-TCP scaffolds portrayed superior structural preservation of the 3D printed bioresorbable scaffolds when compared with implant regions with limited or no bone ingrowth that was associated with disintegrated scaffold structures and multiple strut fractures after 6 months of implantation. This shows that abundance of the newly regenerated bone ensured robust functional participation of the mineralized tissue in the load bearing/sharing dynamics to preserve the structure of implanted bioresorbable scaffolds.

The failure of single-layered PECs to ensure complete interbody spinal fusion in this porcine ALIF model underlines the determinant role of carrier material properties play in the potency of loaded rhBMP-2 as previously reported.[21,27] This finding also underlines the critical

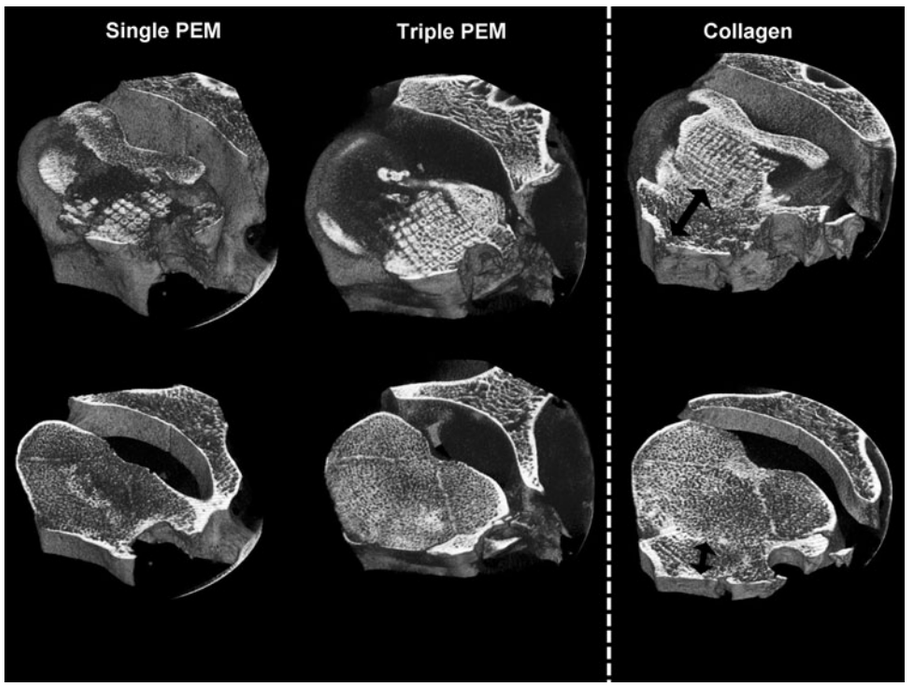

FIG. 7. Three-dimensionally reconstructed images projecting axial views at the level of mPCL-TCP implants (upper panel) and caudal to implants (lower panel). Notice excessive bone growth (heterotopic ossification) beyond the outer border of mPCL-TCP implant (double-headed arrow) only in the collagen group.

importance of bone grafts and/or bone graft substitutes in driving spinal fusion in humans and in large animals. This therefore brings to light the importance of large-animal models in preclinical evaluations as single-layered PECs evaluated previously were able to deliver rhBMP-2 that induced consistent posterolateral spinal fusion in rodents.[13, 17]

In this study, negatively charged heparin interacted with PLL, a positively charged polyamino acid (via electrostatic, Coulomb, interaction), to form PEC deposits as matrices suitable for rhBMP-2 sequestration and immobilization. This self-assembled polyelectrolyte matrix could be tailored to deliver rhBMP-2 and produce comparable, if not superior, interbody spinal fusion when compared to absorbable collagen sponges. The main functional difference between PEC matrix and absorbable collagen sponge as protein carriers is that PECs could be easily tailored to enhance rhBMP-2 sequestration (Figs. 1 and 2D). Besides, immobilized protein within PEC matrices has been reported to exhibit flexible protein conformation and this could further modulate protein release and support protein bioactivity.[13,17,20] In addition, PEC is a synthetic matrix that offers a key advantage over collagen sponges (commonly derived from animal sources) with respect to elimination of risk of immunogenicity. However, it should be noted that direct

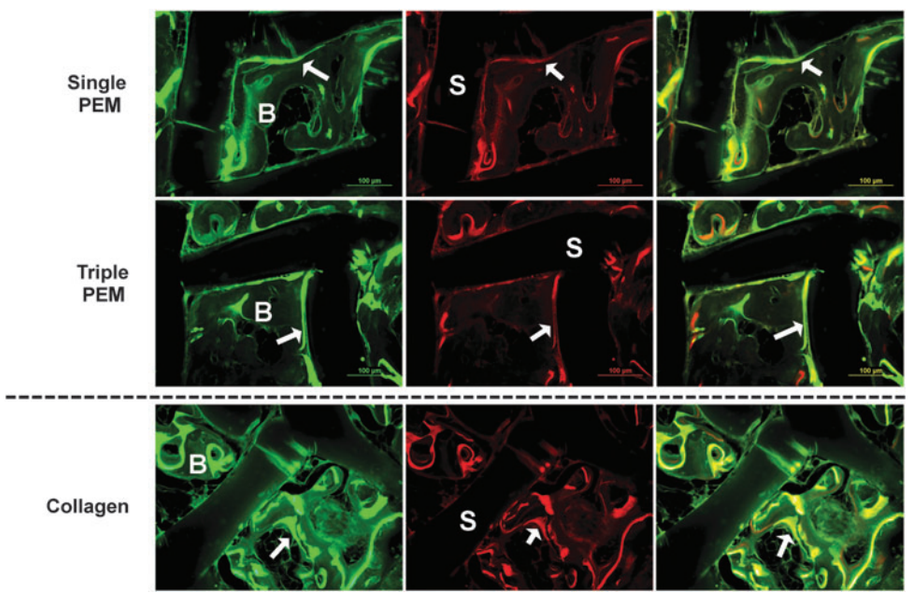

FIG. 8. Double-fluorochrome injection with calcein (green) and alizarin (red) revealed the location of osteoid tissue (arrows) relative to mature bone (B) and mPCL-TCP scaffold struts (S) after 6 months. Notice that osteoid deposition and remodeling activities (white arrows) were predominantly located on the surface of the mPCL-TCP struts in both the PEC groups while collagen matrix carriers showed diffused bone formation in the pore spaces of the scaffold. Color images available online at www.liebertpub.com/tea

implantation of positively charged polyamino acids has a potential to incite *in vivo* inflammation depending on chemical formulation, molecular weight, amount implanted, and, therefore, charge density at implantation.[28,29] Therefore, neutralization of the noninteracted PLL was important in this study and this was effectively achieved by heparin as confirmed on zeta potential measurements (Fig. 2).

While *in vitro* characterization confirmed intact templates during PEC build-up, we observed exfoliation of PEC-protein layers as a membrane after repeated cycles of incubation in solutions of oppositely charged polyelectrolyte (Fig. 1). Despite this peeling off of PECs from alginate surfaces, a physical membrane could still be observed, indicating that the interaction of PLL with heparin may be more stable than that between PLL and alginate, which is consistent with previous report.[30]

Finally, the synthetic construct described here integrates other conceptual advantages in growth factor delivery and bone tissue engineering. The use of noncovalent self-assembly of a polyamino acid (PLL) and a natural ECM GAG molecule (heparin) in PEC build-up could inherently act to provide stability, controlled release, and adjuvant therapeutic effects for several other delicate growth factors besides BMP-2.[31,32] Additionally, the use of microbeads as templates in this approach could enable tuning of sizes to provide larger surface area for heparin (and therefore larger reservoir for growth factors), while the customization of bioresorbable mPCL-TCP using computer-aided design and fused deposition modeling techniques offer versatility for implant design.

Conclusions

Self-assembled PECs spontaneously sequester rhBMP-2 from solution and immobilize the bioactive growth factor for therapeutic application in a clinically relevant bone defect volume. We observed the dependence of rhBMP-2 sequestration efficiency on the amount of heparin within the PEC layers. More importantly, this study clearly shows gross clinical as well as microstructural evidence of the influence of PEC matrices over the extent of heterotopic ossification and morphological bone deposition pattern when compared to collagen sponge carriers in a large-animal model. From a clinical perspective, polyelectrolyte self-assembly could be an alternative delivery platform that would overcome some of the concerns and limitations associated with rhBMP-2 delivery on collagen sponges in the healing of large bone-defect volumes. We anticipate that this synthetic matrix could be adopted in other tissue engineering applications as well as in studies that evaluate growth factor–synthetic matrix interactions.

Acknowledgments

The authors would like to thank Chan Wai Kam, Julee, Ramruttun Amit Kumarsing, and Khoo Hock Hee for their assistance with specimen preparation and technical support. This work was supported by a grant from the Biomedical Research Council (BMRC) A*Star Singapore. S.-A.A., J.G., and H.-K.W. designed research; S.-A.A. and W.M.R.L. performed research and analyzed data; and S.-A.A. and W.M.R.L. wrote the article.

Disclosure Statement

No competing financial interests exist.

References

1. Carragee, E.J., Hurwitz, E.L., and Weiner, B.K. A critical review of recombinant human bone morphogenetic protein-2 trials in spinal surgery: emerging safety concerns and lessons learned. Spine J **11,** 471, 2011.
2. Schwarz, C., Wulsten, D., Ellinghaus, A., Lienau, J., Willie, B.M., and Duda, G.N. Mechanical load modulates the stimulatory effect of BMP2 in a rat nonunion model. Tissue Eng Part A **19,** 247, 2013.
3. Smucker, J.D., Rhee, J.M., Singh, K., Yoon, S.T., and Heller, J.G. Increased swelling complications associated with off-label usage of rhBMP-2 in the anterior cervical spine. Spine **31,** 2813, 2006.
4. Seeherman, H., Wozney, J., and Li, R. Bone morphogenetic protein delivery systems. Spine **27,** S16, 2002.
5. Haidar, Z.S., Hamdy, R.C., and Tabrizian, M. Delivery of recombinant bone morphogenetic proteins for bone regeneration and repair. Part A: current challenges in BMP delivery. Biotechnol Lett **31,** 1817, 2009.
6. Crouzier, T., Szarpak, A., Boudou, T., Auzely-Velty, R., and Picart, C. Polysaccharide-blend multilayers containing hyaluronan and heparin as a delivery system for rhBMP-2. Small **6,** 651, 2010.
7. Crouzier, T., Fourel, L., Boudou, T., Albiges-Rizo, C., and Picart, C. Presentation of BMP-2 from a soft biopolymeric film unveils its activity on cell adhesion and migration. Adv Mater **23,** H111, 2011.
8. Reddi, A.H. Morphogenesis and tissue engineering of bone and cartilage: inductive signals, stem cells, and biomimetic biomaterials. Tissue Eng **6,** 351, 2000.
9. Bramono, D.S., Murali, S., Rai, B., Ling, L., Poh, W.T., Lim, Z.X., *et al.* Bone marrow-derived heparan sulfate potentiates the osteogenic activity of bone morphogenetic protein-2 (BMP-2). Bone **50,** 954, 2012.
10. Zhao, B., Katagiri, T., Toyoda, H., Takada, T., Yanai, T., Fukuda, T., *et al.* Heparin potentiates the *in vivo* ectopic bone formation induced by bone morphogenetic protein-2. J Biol Chem **281,** 23246, 2006.
11. Jeon, O., Kang, S.W., Lim, H.W., Hyung Chung, J., and Kim, B.S. Long-term and zero-order release of basic fibroblast growth factor from heparin-conjugated poly (L-lactide-co-glycolide) nanospheres and fibrin gel. Biomaterials **27,** 1598, 2006.
12. Macdonald, M.L., Samuel, R.E., Shah, N.J., Padera, R.F., Beben, Y.M., and Hammond, P.T. Tissue integration of growth factor-eluting layer-by-layer polyelectrolyte multilayer coated implants. Biomaterials **32,** 1446, 2011.
13. Abbah, S.A., Liu, J., Goh, J.C., and Wong, H.K. Enhanced control of in vivo bone formation with surface functionalized alginate microbeads incorporating heparin and human bone morphorgenic protein-2. Tissue Eng Part A **19,** 350, 2013.
14. Litten-Brown, J.C., Corson, A.M., and Clarke, L. Porcine models for the metabolic syndrome, digestive and bone disorders: a general overview. Animal **4,** 899, 2010.
15. Pearce, A.I., Richards, R.G., Milz, S., Schneider, E., and Pearce, S.G. Animal models for implant biomaterial research in bone: a review. Eur Cell Mater **13,** 1, 2007.
16. Li, H., Zou, X., Springer, M., Briest, A., Lind, M., and Bunger, C. Instrumented anterior lumbar interbody fusion with equine bone protein extract. Spine **32,** E126, 2007.

17. Abbah, S.A., Liu, J., Lam, R.W., Goh, J.C., and Wong, H.K. *In vivo* bioactivity of rhBMP-2 delivered with novel polyelectrolyte complexation shells assembled on an alginate microbead core template. J Control Release **162,** 364, 2012.
18. Wang, M., Abbah, S.A., Hu, T., Toh, S.Y., Lam, R.W., Goh, J., *et al.* Minimizing the severity of rhBMP-2 induced inflammation and heterotopic ossification with a polyelectrolyte carrier incorporating heparin on microbead templates. Spine 2013.
19. Chu, H., Johnson, N.R., Mason, N.S., and Wang, Y. A [polycation:heparin] complex releases growth factors with enhanced bioactivity. J Control Release **150,** 157, 2011.
20. Abbah, S.A., Lam, C.X., Hutmacher, D.W., Goh, J.C., and Wong, H.K. Biological performance of a polycaprolactone-based scaffold used as fusion cage device in a large animal model of spinal reconstructive surgery. Biomaterials **30,** 5086, 2009.
21. Abbah, S.A., Lam, C.X., Ramruttun, A.K., Goh, J.C., and Wong, H.K. Fusion performance of low-dose recombinant human bone morphogenetic protein 2 and bone marrow-derived multipotent stromal cells in biodegradable scaffolds: a comparative study in a large animal model of anterior lumbar interbody fusion. Spine **36,** 1752, 2011.
22. Panjabi, M.M. Biomechanical evaluation of spinal fixation devices: I. A conceptual framework. Spine **13,** 1129, 1988.
23. Sucato, D.J., Hedequist, D., Zhang, H., Pierce, W.A., O'Brien, S.E., and Welch, R.D. Recombinant human bone morphogenetic protein-2 enhances anterior spinal fusion in a thoracoscopically instrumented animal model. J Bone Joint Surg Am **86-A,** 752, 2004.
24. Foldager, C., Bendtsen, M., Nygaard, J.V., Zou, X., and Bunger, C. Differences in early osteogenesis and bone micro-architecture in anterior lumbar interbody fusion with rhBMP-2, equine bone protein extract, and autograft. Bone **45,** 267, 2009.
25. Zara, J.N., Siu, R.K., Zhang, X., Shen, J., Ngo, R., Lee, M., *et al.* High doses of bone morphogenetic protein 2 induce structurally abnormal bone and inflammation *in vivo*. Tissue Eng Part A **17,** 1389, 2011.
26. Shields, L.B., Raque, G.H., Glassman, S.D., Campbell, M., Vitaz, T., Harpring, J., *et al.* Adverse effects associated with high-dose recombinant human bone morphogenetic protein-2 use in anterior cervical spine fusion. Spine **31,** 542, 2006.
27. Abbah, S.A., Lam, C.X., Ramruttun, K.A., Goh, J.C., and Wong, H.K. Autogenous bone marrow stromal cell sheets-loaded mPCL/TCP scaffolds induced osteogenesis in a porcine model of spinal interbody fusion. Tissue Eng Part A **17,** 809, 2011.
28. Morgan, D.M., Larvin, V.L., and Pearson, J.D. Biochemical characterisation of polycation-induced cytotoxicity to human vascular endothelial cells. J Cell Sci **94(Pt 3),** 553, 1989. ◀AU6
29. de Vos, P., Spasojevic, M., de Haan, B.J., and Faas, M.M. The association between *in vivo* physicochemical changes and inflammatory responses against alginate based microcapsules. Biomaterials **33,** 5552, 2012.
30. Varghese, M.S., Hildebrandt, D., Glasser, D., Rubin, D.M., and Crowther, N.J. The effect of poly-L-lysine/alginate bead membrane characteristics on the absorption of heparin. Artif Cells Blood Substit Immobil Biotechnol **37,** 13, 2009.
31. Damon, D.H., Lobb, R.R., D'Amore, P.A., and Wagner, J.A. Heparin potentiates the action of acidic fibroblast growth factor by prolonging its biological half-life. J Cell Physiol **138,** 221, 1989.
32. Fatma, N., Singh, D.P., Shinohara, T., and Chylack, L.T., Jr. Heparin's roles in stabilizing, potentiating, and transporting LEDGF into the nucleus. Invest Ophthal Vis Sci **41,** 2648, 2000.

Address correspondence to: ◀AU4
Hee-Kit Wong, MD
Department of Orthopaedic Surgery
Yong Loo Lin School of Medicine
National University of Singapore
NUHS Tower Block
1E Kent Ridge Rd.
Singapore 119228
Singapore

E-mail: heekit_wong@nuhs.edu.sg

Received: September 20, 2013
Accepted: December 17, 2013
Online Publication Date:

AUTHOR QUERY FOR TEA-2013-0593-VER9-ABBAH_1P

AU1: Please note that gene symbols in any article should be formatted per the gene nomenclature. Thus, please make sure that gene symbols, if any in this article, are italicized.
AU2: Please review all authors' surnames for accurate indexing citations.
AU3: Please mention the degrees of authors Wing Moon Raymond Lam, Tao Hu, and James Goh.
AU4: Please confirm authors' affiliations and address of correspondence.
AU5: Symbol '' $\approx$ '' has been changed to ''='' in the text ''Deposition of…($\zeta = -50$).'' Please confirm.
AU6: Ref. 28 has been deleted as it was a duplicate of Ref. 13, and Ref. citations in the text have been renumbered accordingly. Please check.
AU7: Please mention the significance of ''*'' and ''**'' in Figure 2 legend.
AU8: The symbol ''**'' is missing in Figure 6. Please check.